Proceedings of the 10th World Congress on Mechanical, Chemical, and Material Engineering (MCM'24)
Barcelona, Spain –August 22-24, 2024
Paper No. HTFF 136
DOI: 10.11159/htff24.136

A 3D-DDES Numerical Simulation of Jet Blowing as a Power Enhancement Technique Applied to a Wind Turbine with S809 Profile

Giacomo Tosatti[1], Luca Manni[2], Ivano Petracci[1*]

(1), Department of Industrial Engineering, University of Rome "Tor Vergata", via del Politecnico n.1, 00133 Rome, Italy
(2), Cecom srl, Via Tiburtina, km 18,700, 00012 Guidonia Montecelio, Rome, Italy
giacomo.tosatti@students.uniroma2.eu; l.manni@cecomweb.com; ivano.petracci@uniroma2.it (*corresponding author)

Abstract **-** The aerodynamic performance of the NREL Phase VI wind turbine is investigated through the use of the blade element momentum (BEM) theory and computational fluid dynamics (CFD). The baseline configuration, consisting of an S809 airfoil, is modified to employ trailing edge blowing technology, an active circulation control technique known as Coanda Jet. Calculations are performed via 3D Delayed Detached Eddy Simulation (DDES) to solve the three-dimensional flow structures over the airfoil correctly. A preliminary campaign of simulations is first conducted for a wide range of angles of attack from $\alpha = 0°$ to $\alpha = 20°$ on an airfoil with chord $c = 0.482$ m with a wind speed equal to 29.3 m/s, which corresponds to the chord at 75% of the blade radius and the relative wind velocity it experiences respectively. Results are confronted with experiments to validate the model. Once mesh fidelity is proven, five different radial positions along the blade are considered and simulations are performed with and without jet blowing to prove its efficiency. Results show that lift and thrust force both increase, enhancing net power generated by the wind turbine, which is calculated via BEM.

Keywords**:** Wind Turbine; S809 Airfoil; Circulation Control; Jet Blowing; 3D-DDES simulation; Power Enhancement

1. Introduction

Fossil fuels have always been humanity's main source of energy power. However, due to their finite nature and the increasing necessity of lowering CO2 emissions coupled with a growing demand for energy production, researchers focused their attention on new sources such as renewables. Among all the environmentally friendly alternatives, wind energy stands as the second most prominent, preceded only by solar power [1]. As of June 2023, global installed wind power capacity reached 976 GW, and by the end of the year, an additional growth to 1045 GW is expected, with China and the USA composing more than 50% of it, followed by a large number of European countries [2]. Given the extensive use of wind turbines and the consequent investment in the order of billions of dollars [3], it is only evident why intensive efforts have been undertaken to maximize energy conversion efficiency, an objective satisfied by the employment of the so-called passive and active flow control devices, whose purpose is increasing the lift force which is in turn strictly related to power. The former consists of a simple modification of the airfoil geometry (flaps, slats, vortex generators), while the latter implies the expense of power provided by an external source, such as a compressor, to further increase the generated one: it is the case of jet blowing, or Coanda jet. This technology was born in aeronautics [4] and has been widely studied, as far as jet thickness, momentum and trailing edge radius are concerned by Djojodihardjo et al. [5] for wind turbine applications. It consists of the injection of pressurized fluid along the suction side, usually close to the airfoil's trailing edge, with the goal of re-energizing the boundary layer to resist typical adverse pressure gradients delaying stall ([6],[7]) and, most importantly, forcing the surrounding fluid to adhere to the curved surface, increasing the circulation of velocity and thus lift force, as explained by the Kutta-Žukovskij's theorem [8]. However, it must be noted that implementing trailing edge blowing implies its rounding, leading to an amplification of drag force, a problem that can be mitigated by designing its lower part as flat as possible as suggested by Englar in [9]. Since airfoil geometry plays a fundamental role as well, researchers have conducted numerous studies on its optimization to pursue a compromise between lift and drag generation. An example is the S809 airfoil, designed by Somers in 1997 explicitly for wind energy application and tested in the low-turbulence wind tunnel of the Delft University of Technology Low-Speed Laboratory [10]. The specified airfoil was subsequently integrated into the NREL Phase-VI wind turbine, specifically devised for experimental investigations, and tested by Hand et al. [11] in the NASA Ames Research Center's wind tunnel, characterized by a 24.4 m x 36.6 m test section and a maximum wind speed of 50 m/s. This work seeks to demonstrate the attractiveness of blowing technology. As outlined in the abstract, the initial phase involves conducting a

series of preliminary 3D simulations on the airfoil at 75% of the blade radius without the jet, aiming to demonstrate mesh reliability and results will then be confronted with those of Somers for validation. The investigation will then extend to five different radial positions along the blade, through the use of Blade Element Momentum theory (BEM), generated power will be evaluated in both jet-off and jet-on configurations to highlight its increase and prove the energy efficiency of the lift-increasing method.

2. Numerical methodology

2.1. Governing equations

The core equations descriptive of the problem are the first and second Navier-Stokes equations, nominally conservation of mass and momentum. Assuming the fluid to be incompressible, they can be written in their instantaneous form respectively as:

$$\frac{\partial u_i}{\partial x_i} = 0 \tag{1}$$

$$\frac{\partial u_i}{\partial t} + u_j \frac{\partial u_j}{\partial x_j} = -\frac{1}{\rho}\frac{\partial \mathrm{p}}{\partial x_i} + \nu \frac{\partial^2 u_i}{\partial x_i \, \partial x_j} \tag{2}$$

Where x_i represents the i-th coordinate, u_i the i-th instantaneous velocity component written in a Cartesian reference frame, p is the instantaneous static pressure, ρ the density of the fluid and ν the kinematic viscosity. It is well known that the flow regime transitions from laminar to turbulent after a certain value of the Reynolds number, defined in Eq. (3):

$$\mathrm{Re} = \frac{\mathrm{uL}}{\nu} \tag{3}$$

Where L is a characteristic dimension of the problem. This transition implies random changes in the instantaneous flow variables and, according to the turbulence description given by Kolmogorov in [12], it is only evident why a direct approach to solving the aforementioned equations via Direct Numerical Simulation (DNS) is deemed impractical, primarily due to the substantial time and computational resources required. A well-established method consists of performing the Reynolds average and so obtaining the Unsteady Reynolds-Average Navier-Stokes equations (URANS):

$$\frac{\partial U_i}{\partial x_i} = 0 \tag{4}$$

$$\frac{\partial U_i}{\partial t} + U_j \frac{\partial U_i}{\partial x_j} = -\frac{1}{\rho}\frac{\partial P}{\partial x_i} + \frac{\partial}{\partial x_j}\left(\nu \frac{\partial U_i}{\partial x_j} - \overline{u_i' u_j'}\right) \tag{5}$$

Where U_i and P_i are the mean values of velocity and pression and the additional term $-\overline{u_i' u_j'}$, when multiplied by the density ρ, is the apparent Reynolds stess added by the fluctuations of velocity in the mean flow. This term adds new unknown variables, hence the need to model it through the introduction of new equations. Another technique is the Large Eddy Simulation (LES), consisting of a direct numerical solution of the large eddies and the modelling of smaller ones with a Sub-Grid Scale model, since they are easier to predict thanks to their almost-isotropic nature: this filtering operation is done through a spatial filter (i.e. mesh resolution) [14]. It is noteworthy that, while not as demanding in terms of time and resources as DNS, this approach is still relatively costly, hence why its use is mainly limited to academic research. This problem arises from the filtering operation itself, since wall-parallel grid dimensions become as crucial as wall-normal ones; a problem URANS does not encounter. In the present work, a DES approach is chosen. Developed by Spalart in 1997 [13] and known as DES97, it consists of a hybrid RANS-LES approach: URANS is applied in the boundary layer where an onerous grid resolution would be required to solve the smaller scales born through the wall-flow interactions, modelling them instead; LES is used away from the wall. This method is, however, highly grid-dependent: a mesh fine enough to enter the boundary layer but not fine enough for accurate computation of the Reynolds stresses can cause the so-called Modelled Stress Depletion [15], resulting in an artificial flow detachment [16]. The Delayed Detached Eddy Simulation was so proposed by Spalart et al. in [17] to avoid this issue, a result obtained by modifying the definition of the length scale as shown below. In this work the k − ω SST turbulence model proposed by

Menter [18] is employed to model the boundary layer. The transport equations of the turbulent kinetic energy k and the rate of dissipation ω necessary to model the term $-\overline{u_i' u_j'}$ in the URANS part are respectively:

$$\frac{\partial k}{\partial t} + U_j \frac{\partial k}{\partial x_j} = P_k - \frac{k^{3/2}}{L_{DDES}} + \frac{\partial}{\partial x_j}\left[(\nu + \sigma_k \nu_T)\frac{\partial k}{\partial x_j}\right] \tag{6}$$

$$\frac{\partial \omega}{\partial t} + U_j \frac{\partial \omega}{\partial x_j} = \alpha S^2 - \beta \omega^2 + \frac{\partial}{\partial x_j}\left[(\nu + \sigma_\omega \nu_T)\frac{\partial \omega}{\partial x_j}\right] + 2(1 - F_1)\sigma_{\omega 2}\frac{1}{\omega}\frac{\partial k}{\partial x_i}\frac{\partial \omega}{\partial x_i} \tag{7}$$

Where L_{DDES} is the integral length scale, dependent on the turbulent length scale of the k − ω SST L_t and the maximum grid dimension Δ_{max}, defined in Eq. (8); ν_T is the turbulent kinematic viscosity and P_k is the production limiter, whose purpose is to avoid excessive build-up of turbulent kinetic energy near stagnation points at the leading edge of an airfoil:

$$L_{DDES} = L_t - f_d max(0, L_t - C_{DDES}\Delta_{max}) \tag{8}$$

with this length scale definition, when f_d is 1 the model behaves as a LES and transitions to a RANS model when f_d is 0. More insights about the variables and constants in Eq. (6), (7), (8) can be found in [19].

2.2. Grid generation

The original S809 airfoil with a chord length of 482 mm has been modified to integrate the Coanda technology. The jet is placed at 95% of the chord *c* and its thickness t_j is selected to obtain a ratio $\frac{t_j}{c} = 0.2\%\ c$. The trailing edge was subsequently shaped by rounding and truncating to create a semi-circumference so that $\frac{t_j}{R_{TE}} = 0.2$, where R_{TE} is the trailing edge's radius, leaving the pressure side's part flat as recommended by Englar in [4]. Given this particular geometry, an O-mesh block strategy, realized with Ansys ICEM meshing software, has been chosen to minimize element skewness and ensure orthogonality near the blunt edges of the trailing edge. It consists of a circumference of radius R = 50c centered on the airfoil's leading edge to guarantee independence of the turbulent quantities concerning the inlet boundary condition. Similarly, this extension also ensures a correct development of the wake, avoiding contaminations arising from the pressure imposed on the outlet boundary condition. Then, an auxiliary O-grid with a radius of r=4c is created to obtain a finer mesh in proximity to the airfoil and a controlled growth ratio. The mesh is then extruded in the spanwise direction for a length of 0.5*c*. A velocity $v = 29.3$ m/s is imposed on the inlet, and a gauge pressure p = 0 Pa is on the outlet. The velocity mentioned above guarantees a Reynolds number evaluated with the chord $Re \approx 0.9 \cdot 10^6$, hence the choice to use Somers' results as a benchmark for validation given that his Reynolds number, equal to $Re = 1 \cdot 10^6$, is the closest available in literature to the one adopted in this work. A translational periodic boundary condition is imposed on the front and back faces of the domain to emulate an "infinite" blade. The height of the first cell near the profile is fixed to achieve a $y+ < 1$ and the growth ratio is chosen to be ≤ 1.15. It should be noted that two extra blocks are needed to mesh the trailing edge and, given its particular geometry, it was necessary to transform the last square block into a triangular one as can be seen in Fig. 3c. The grid resolution study has been carried out for an angle of attack α=14° for three different meshes, whose details are reported in Tab. 1, while a closeup can be found in Fig. 3a and Fig. 3b. Results of the three simulations are instead reported in Tab. 2. The medium-resolution mesh was selected for the remaining simulations due to the close resemblance of the lift coefficients C_L between the medium and the fine resolution. The jet canal is later modelled on the pre-existing mesh by adding a new block whose length is ten times the thickness and with its right edge coinciding with the slot connecting the suction side with the rounded trailing edge. It is then segmented with 70x70x64 points in the streamwise, normal, and spanwise directions, respectively.

The time step adopted is $\Delta t = 1 \cdot 10^{-4}\ s$ to guarantee CFL<1 at least in the LES region, while keeping it < 5 in the RANS region. As far as spatial discretization is concerned, turbulent kinetic energy and specific dissipation rate are treated with a Second Order Upwind scheme, while momentum is treated with a Bounded Central Differencing scheme. The flow is assumed incompressible, hence the decision to treat pressure-velocity coupling with the SIMPLE algorithm [20]. Lastly, time is discretized via a Bounded Second Order Implicit scheme. Every simulation, carried out in Ansys FLUENT, is run for 1.6s to eliminate any influence of the initialization conditions, following which average quantities are monitored for an additional 3.2s, corresponding to two domain laps.

Tab. 1: Details of the three meshes for the baseline S809 airfoil.

Parameters	Coarse	Medium	Fine
Normal points in R	40	50	60
Normal points in r	100	120	140
Growth ratio in R	1.1	1.1	1.1
Growth ratio in r	1.15	1.1	1.05
Wrap-around points	340	520	660
Leading edge spacing/c	0.005	0.0025	0.001
Spanwise points	64	64	64
y^+	< 1	< 1	< 1

Tab. 2: Comparison of the aerodynamic coefficients for the three meshes.

Results	Coarse	Medium	Fine	Experiment [10]
C_L	0.957	0.998	1.012	1.055
C_D	0.0932	0.0793	0.0764	0.0828

Once mesh fidelity is proven, it is both upscaled and downscaled to achieve a chord length equal to those at radial positions along the turbine blade, namely $\frac{r}{R} = 0.3, 0.47, 0.63, 0.8, 0.95$, while the spanwise length is kept constant. More simulations are run with jet both off and on to estimate the generated power and its increase.

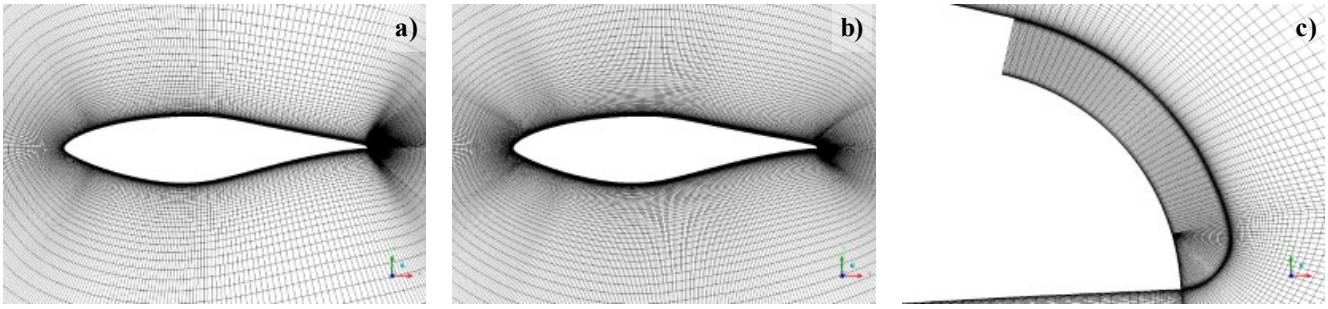

Fig. 1: Close-up of the medium and fine mesh with detailed view of the trailing edge. a) Medium mesh. b) Fine mesh. c) Detail of the mesh near the trailing edge.

3. Results

3.1. Mesh validation

A wide range of angles of attack has been tested, spanning from 0° to 20° in increments of two. As can be seen from Fig. 2, the lift curve closely follows Somers' in shape; the discrepancy is found in the intensity of C_L. The author believes this is caused by the difference in Reynolds number between the simulations presented in this work and, most importantly, by the effect of wall-interference typical of subsonic wind tunnels [21]. However, given the nearly identical slope in the linear part of the curve from α = 0° to α = 6°, the similarity in the first-stall region from α = 8° to α = 12° as well as the subsequent recovery and deep-stall, results were deemed satisfactory. Fig. 3 shows the comparison of pressure coefficients for four of the tested angles.

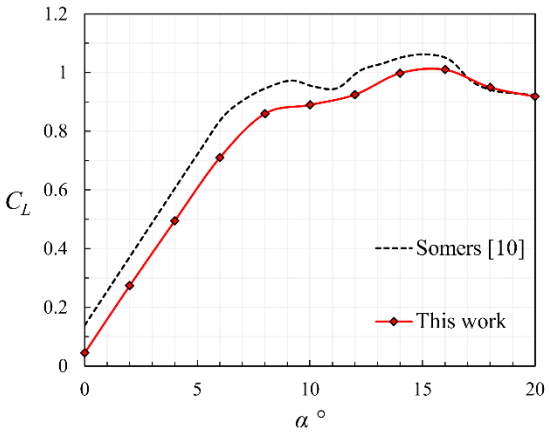

Fig. 2: Lift curve of carried out simulations. Re = $0.9 \cdot 10^6$

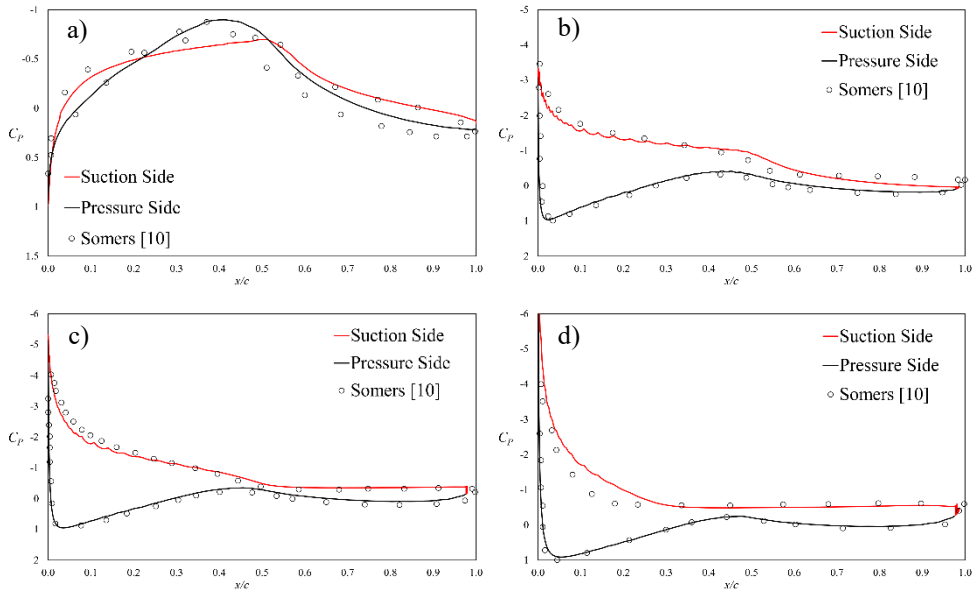

Fig. 3: Pressure coefficients for four different angles of attack. a) α = 0°, b) α = 10°, c) α = 14° and d) α = 20°.

3.2. Blade Element Momentum theory

This theory is obtained from Blade Element Theory, which introduces momentum and considers the blade's rotation; the rotor is simplified to a series of independent annular rings. It should be noted that this theory overpredicts power generation because it does not account for wake expansion and tip losses. Fig. 4 clearly shows the correlation between lift L and drag D forces with the torque T_q and thrust T_h, hence the definition of torque and thrust coefficients C_{Tq} and C_{Th} in Eq. (9) and Eq. (10).

$$C_{Tq} = C_L \sin(\alpha + \theta) - C_D \cos(\alpha + \theta) \tag{9}$$

$$C_{Th} = C_L \cos(\alpha + \theta) + C_D \sin(\alpha + \theta) \tag{10}$$

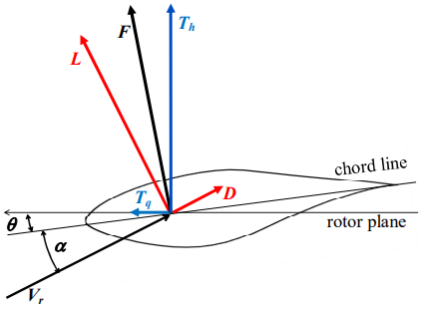

Fig. 4: Aerodynamics forces acting on the S809 airfoil and their decomposition [22]

Where θ is the sum of pitch and yaw angle. The torque produced by the infinitesimal element can be evaluated from Eq. (11):

$$dT = \frac{1}{2}\rho c C_{\mathrm{Tq}} V_r^2 r dr \tag{11}$$

Where V_r is the relative velocity experienced by the blade, coinciding with the inlet velocity, c the local chord length and dr the infinitesimal distance along the radius of the blade r. By introducing the rotational velocity ω, considered constant for simplicity's sake, generated power can be estimated from Eq. (12):

$$P = \omega \int_{r_0}^{R} \frac{1}{2}\rho c C_{\mathrm{Tq}} V_r^2 r dr \tag{12}$$

Thus, a series of 3D simulations are carried out on five radial positions of the NREL Phase-VI wind turbine, whose geometrical properties are taken from [11] and shown in Tab. 3. The chosen wind speed V is equal to 7 m/s and relative velocity V_r is found from Eq. (13).

Tab. 3: Geometrical properties and experienced velocity of the five sections.

r [m]	r/R	c [m]	V_r [m/s]	ω [rpm]	α [°]	ϑ [°]
1.51	0.3	0.711	13.35	72	14.31	17.29
2.343	0.47	0.627	19.14	72	13.73	7.71
3.172	0.63	0.543	24.89	72	12.18	4.15
4.023	0.8	0.457	31.13	72	10.38	2.62
4.78	0.95	0.381	36.69	72	9.47	1.53

$$V_r = \sqrt{V^2 + (\omega r)^2} \tag{13}$$

When on, the jet velocity is assigned so that the coefficient of jet momentum $C\mu = 0.004$, which is defined as:

$$C_\mu = \frac{U_\mathrm{j}^2 A_\mathrm{j}}{\frac{1}{2} U_{\mathrm{tip}}^2 A_{\mathrm{ref}}} \tag{14}$$

where U_j and A_j are the jet's velocity and exit area, respectively, while U_{tip} and A_{ref} are the velocity at the blade's tip and reference planform area. The jet's thickness varies with the radial coordinate r but follows the same ratio $\frac{t_j}{c} = 0.2\%\ c$. The power P_j required to operate the jet is estimated from Eq. (15) assuming a compression efficiency $\eta_c = 0.85$. The power percentage change is determined from Eq. (16), considering that for the given case $P_\mathrm{j} = 241$ W:

$$P_\mathrm{j} = \frac{\frac{1}{2}\rho_\mathrm{j} A_\mathrm{j} U_\mathrm{j}^3}{\eta_\mathrm{c}} \tag{15}$$

$$\frac{\Delta P}{P} = \frac{\left(P - P_{jet}\right) - P_{baseline}}{P_{baseline}} \tag{16}$$

Tab. 4: Computed torque, power and experimental data.

	T [Nm]	P [kW]	$\Delta P/P$ [%]
Experiment [11]	803.6	6.06	/
Jet off	963.5	7.26	/
Jet on	1094.1	8.00	+10.2

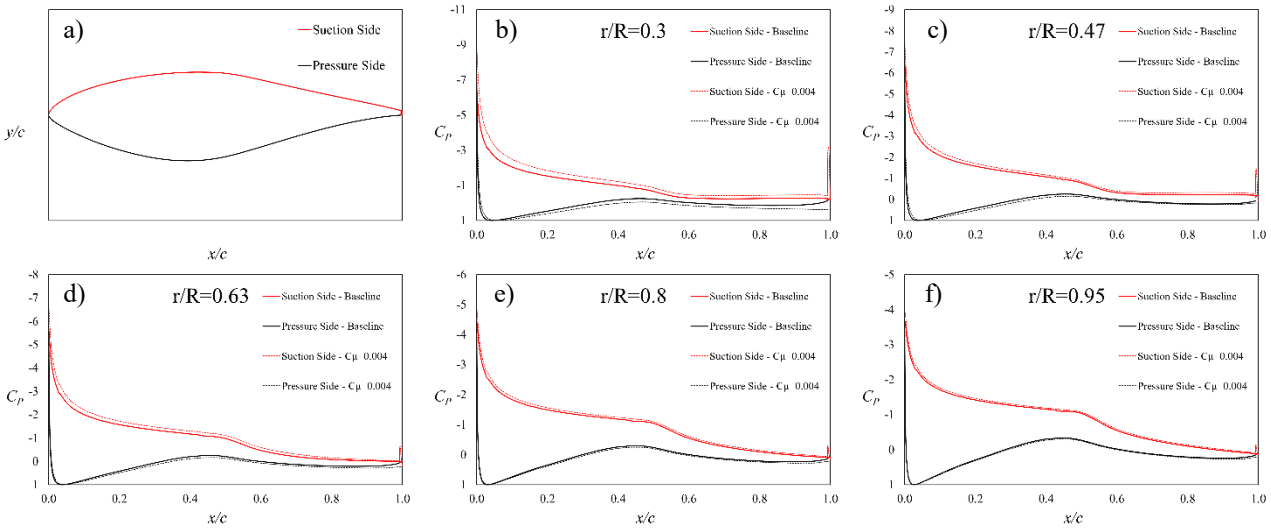

Fig. 5: S809 airfoil and pressure profiles along a-dimensionalized chord length: baseline and jet on configurations.

Computed torque and power are reported in Tab. 4. It is evident how BEM overestimates key parameters; however, some interesting remarks can be made. Implementation of the Coanda technology improved power generation by a margin of 10.2% thanks to a substantial increase in lift force coupled with a slight increase in drag force, typical of jet blowing. This aspect is highlighted in Fig. 5, where the pressure coefficients C_P of the five tested sections are shown for both jet-off and jet-on configurations. Fig. 5b displays the one closer to the blade root: it is evident how the jet amplifies the area between the two curves, justifying the lift improvement. This effect can also be observed in the middle sections, up to position $\frac{r}{R} = 0.63$ (Fig. 5d). From this point onward (Fig. 5e and Fig. 5f) the baseline curves of both suction and pressure side overlap with their jet-on counterpart, suggesting an almost negligible response to the injected pressurized flow. This can be explained by the increase in velocity experienced by the sections closer to the blade tip, which becomes increasingly similar to the jet's velocity. Consequently, this reduces the difference in momentum between the two, hence flow deflection, which implies, in turn, a trivial effect on circulation.

4. Conclusion

A campaign of 3D Delayed Detached Eddy Simulation has been conducted on a series of sections along the blade, based on the S809 airfoil, of the NREL Phase-VI wind turbine. The work aimed to show how the injection of a pressurized flow near the airfoil's leading edge ($\frac{x}{c} = 0.95\%$) would increase its performance and, most importantly, assess the energy

efficiency of the proposed technology. The section at 75% of the blade radius was first simulated and results were confronted with Somer's [10] for mesh validation. Five radial positions are then considered, and the power generated is estimated using the BEM theory. Results have shown how this technology improves turbine performance at very little expense. However, the most substantial variations are found near the blade root and in the middle sections. Future developments might include the introduction of different slots along the blade with varying momentum (i.e. modulating velocity) to fully exploit the jet along the whole rotor radius, further improving performances.

References

[1] International Energy Association. (2023, June). [Online]. Available: https://www.iea.org/reports/renewable-energy-market-update-june-2023/executive-summary

[2] World Wind Energy Association. (2023, 7 November). [Online]. Available: https://wwindea.org/wwea-half-year-report-2023-additional-momentum-for-windpower-in-2023/

[3] REN21. 2023. Renewables 2023 Global Status Report collection, Renewables in Energy Supply

[4] R. J. Englar, "Circulation Control for High Lift and Drag Generation on STOL Aircraft," *Journal of Aircraft*, vol. 12, no. 5, pp. 457–463, May 1975, doi: https://doi.org/10.2514/3.59824.

[5] H. Djojodihardjo, M. F. Abdul Hamid, A. A. Jaafar, S. Basri, F. I. Romli, F. Mustapha, A. S. Mohd Rafie and D. L. A. Abdul Majid, "Computational Study on the Aerodynamic Performance of Wind Turbine Airfoil Fitted with Coandă Jet," *Journal of Renewable Energy*, vol. 2013, pp. 1–17, 2013, doi: https://doi.org/10.1155/2013/839319.

[6] D. Greenblatt and I. J. Wygnanski, "The control of flow separation by periodic excitation," *Progress in Aerospace Sciences*, vol. 36, no. 7, pp. 487–545, Oct. 2000, doi: https://doi.org/10.1016/S0376-0421(00)00008-7.

[7] Hanns Müller-Vahl, Christian Navid Nayeri, Christian Oliver Paschereit, and D. Greenblatt, "Dynamic stall control via adaptive blowing," *Renewable Energy*, vol. 97, pp. 47–64, Nov. 2016, doi: https://doi.org/10.1016/j.renene.2016.05.053.

[8] J. Anderson, *Introduction to Flight*. New York, Ny: Mcgraw-Hill Education, 2016.

[9] R. J. Englar, "Circulation control pneumatic aerodynamics: blown force and moment augmentation and modification - Past, present and future," *Fluids 2000 Conference and Exhibit*, Jun. 2000, doi: https://doi.org/10.2514/6.2000-2541.

[10] D. M. Somers, *Design and Experimental Results for the S809 Airfoil*. 1997.

[11] M.M. Hand, D.A. Simms, L.J. Fingersh, D.W. Jager, J.R. Cotrell, S. Schreck and S.M. Larwood, "Unsteady Aerodynamics Experiment Phase VI: Wind Tunnel Test Configurations and Available Data Campaigns," Dec. 2001, doi: https://doi.org/10.2172/15000240.

[12] A. N. Kolmogorov, "A refinement of previous hypotheses concerning the local structure of turbulence in a viscous incompressible fluid at high Reynolds number," *Journal of Fluid Mechanics*, vol. 13, no. 1, pp. 82–85, May 1962, doi: https://doi.org/10.1017/s0022112062000518.

[13] P. R. Spalart, "Comments on the feasibility of LES for wings, and on a hybrid RANS/LES approach," Jan. 1997.

[14] J. SMAGORINSKY, "GENERAL CIRCULATION EXPERIMENTS WITH THE PRIMITIVE EQUATIONS," *Monthly Weather Review*, vol. 91, no. 3, pp. 99–164, Mar. 1963, doi: https://doi.org/10.1175/1520-0493(1963)091%3C0099:GCEWTP%3E2.3.CO;2.

[15] P. R. Spalart, "Strategies for turbulence modelling and simulations," *International Journal of Heat and Fluid Flow*, vol. 21, no. 3, pp. 252–263, Jun. 2000, doi: https://doi.org/10.1016/s0142-727x(00)00007-2.

[16] F. R. Menter, M. Kuntz and R. Langtry, "Ten Years of Industrial Experience with the SST Turbulence Model," Proceedings of the 4th International Symposium on Turbulence, Heat and Mass Transfer, Begell House Inc., West Redding, 2003, pp. 625-632.

[17] P. R. Spalart, S. Deck, M. L. Shur, K. D. Squires, M. Kh. Strelets, and A. Travin, "A New Version of Detached-eddy Simulation, Resistant to Ambiguous Grid Densities," *Theoretical and Computational Fluid Dynamics*, vol. 20, no. 3, pp. 181–195, May 2006, doi: https://doi.org/10.1007/s00162-006-0015-0.

[18] F. Menter, "Zonal Two Equation k-w Turbulence Models For Aerodynamic Flows," *23rd Fluid Dynamics, Plasmadynamics, and Lasers Conference*, Jul. 1993, doi: https://doi.org/10.2514/6.1993-2906.

[19] Fluent, A. N. S. Y. S. (2011). Ansys fluent theory guide. Ansys Inc., USA, 15317, 724-746

[20] S. V. Patankar. Numerical heat transfer and fluid flow. Series in computational methods in mechanics and thermal sciences. Hemisphere Publ. Co, New York, 1980.

[21] K. Duraisamy, W. J. McCroskey, and J. D. Baeder, "Analysis of Wind Tunnel Wall Interference Effects on Subsonic Unsteady Airfoil Flows," *Journal of Aircraft*, vol. 44, no. 5, pp. 1683–1690, Sep. 2007, doi: https://doi.org/10.2514/1.28143.

[22] I. Petracci, L. Manni, M. Angelino, S. Corasaniti, F. Gori, 2019, *"A 2d-Numerical Study on Slot Jet Applied to a Wind Turbine as a Circulation Control Technique",* XII International Conference on Computational Heat, Mass and Momentum Transfer, Series: E3S Web of Conferences Volume 128 (2019), Editor: Mohamad, A. Jan Taler, Ali Cemal Benim EDP Sciences, 2019. , ISBN: 9781510898547